



UNIVERSITY OF LEEDS

This is a repository copy of *Short Terahertz Pulse Generation from a Dispersion Compensated Modelocked Semiconductor Laser*.

White Rose Research Online URL for this paper:

<http://eprints.whiterose.ac.uk/119029/>

Version: Accepted Version

Article:

Wang, F, Nong, H, Fobbe, T et al. (14 more authors) (2017) Short Terahertz Pulse Generation from a Dispersion Compensated Modelocked Semiconductor Laser. *Laser and Photonics Reviews*, 11 (4). 1700013. ISSN 1863-8880

<https://doi.org/10.1002/lpor.201700013>

© 2017 by WILEY-VCH Verlag GmbH & Co. KGaA, Weinheim. This is the peer reviewed version of the following article: F. Wang, H. Nong, T. Fobbe, V. Pistore, S. Houver, S. Markmann, N. Jukam, M. Amanti, C. Sirtori, S. Moumdji, R. Colombelli, L. Li, E. Linfield, G. Davies, J. Mangeney, J. Tignon, S. Dhillon, *Laser & Photonics Reviews* 2017, 11, 1700013., which has been published in final form at <https://doi.org/10.1002/lpor.201700013>. This article may be used for non-commercial purposes in accordance with Wiley Terms and Conditions for Self-Archiving.

Reuse

Items deposited in White Rose Research Online are protected by copyright, with all rights reserved unless indicated otherwise. They may be downloaded and/or printed for private study, or other acts as permitted by national copyright laws. The publisher or other rights holders may allow further reproduction and re-use of the full text version. This is indicated by the licence information on the White Rose Research Online record for the item.

Takedown

If you consider content in White Rose Research Online to be in breach of UK law, please notify us by emailing eprints@whiterose.ac.uk including the URL of the record and the reason for the withdrawal request.

Article type: Original Paper

Short terahertz pulse generation from a dispersion compensated modelocked semiconductor laser

Feihu Wang¹, Hanond Nong¹, Tobias Fobbe², Valentino Pistore¹, Sarah Houver¹, Sergej Markmann², Nathan Jukam², Maria Amanti³, Carlo Sirtori³, Souad Moumdji⁴, Raffaele Colombelli⁴, Lianhe Li⁵, Edmund Linfield⁵, Giles Davies⁵, Juliette Mangeney¹, Jérôme Tignon¹, and Sukhdeep Dhillon^{1,}*

*Corresponding Author: E-mail: sukhdeep.dhillon@lpa.ens.fr

¹Laboratoire Pierre Aigrain, Département de physique de l'ENS, École normale supérieure, PSL Research University, Université Paris Diderot, Sorbonne Paris Cité, Sorbonne Universités, UPMC Univ. Paris 06, CNRS, 75005 Paris, France

²Lehrstuhl für Angewandte Festkörperphysik, Ruhr-Universität Bochum, Universitätsstraße 150, 44780 Bochum, Germany

³Laboratoire Matériaux et Phénomènes Quantiques, Université Paris Diderot, Sorbonne Paris Cité, CNRS-UMR 7162, 75013 Paris, France

⁴ Centre de Nanosciences et de Nanotechnologies, CNRS, Univ. Paris-Sud, Université Paris-Saclay, C2N – Orsay, 91405 Orsay cedex, France

⁵School of Electronic and Electrical Engineering, University of Leeds, Woodhouse Lane, Leeds

Dispersion compensation is vital for the generation of ultrashort and single cycle pulses from modelocked lasers across the electromagnetic spectrum. It is typically based on addition of an extra dispersive element to the laser cavity that introduces a chromatic dispersion opposite to that of the gain medium. To date, however, no dispersion compensation schemes have been successfully applied to terahertz (THz) quantum cascade lasers for short and stable pulse generation in the THz range. In this work, a monolithic on-chip compensation scheme is realized for a modelocked QCL, permitting THz pulses to be considerably shortened from 16ps to 4ps. This is based on the realization of a small coupled cavity resonator that acts as an ‘off resonance’ Gires-Tournois interferometer (GTI), permitting large THz spectral bandwidths to be compensated. This novel application of a GTI opens up a direct and simple route to sub-picosecond and single cycle pulses in the THz range from a compact semiconductor source.

1. Introduction

In the terahertz (THz) frequency range ($\sim 0.5 - 5$ THz), [1] with its proven applications in imaging, [2,3] metrology, [4,5] and non-destructive testing, [6,7] a semiconductor based technology platform for intense and ultrashort pulse generation has yet to be realized. This is in contrast to the optical and near-infrared (NIR) domain where ultrashort pulse generation can be readily achieved in devices such as mode locked semiconductor diodes and vertical external cavity surface emitting lasers (VECSELS). [8–10] Although THz quantum cascade lasers (QCLs) are a foundational semiconductor laser in the THz range, to date, the generation of stable and ultrashort pulses from QCLs has proven to be difficult. These devices, first realized in 2002, [11,12] are one of the only practical semiconductor systems that offers gain in the THz range, [13] where the ‘band structure-by-design’ nature of QCLs allows the frequency, and bandwidth to be entirely engineered. [14] Active mode locking, where the device is electrically modulated at its’ roundtrip, has been extensively applied but the pulses generated so far have been limited to the range of 10ps to 20ps, despite several years of research effort. [15,16] Although THz QCLs with extremely large gain bandwidths have been realized leading to impressive developments in frequency comb generation, [17,18] this has not translated directly into the formation of stable short pulses in the THz range (In general the pulse width is inversely proportional to the spectral bandwidth). [19]

To generate ultrashort pulses from a laser, the following components are required i) a gain medium within a laser cavity; ii) a modelocking mechanism such as the fast modulation of the losses or gain at the cavity round-trip and iii) dispersion compensation. The first two points have been widely investigated for THz QCLs, as well as for MIR QCLs. [20,21] Regarding the third point, dispersion indicates that the refractive index varies with frequency and is undesirable for short pulse generation. It is often characterized by the group velocity dispersion

(GVD) or equivalently the group delay dispersion (GDD). ($\text{GDD} = \text{GVD} \times L$ where L is the length of the material). [22] This parameter is critical in ultrafast lasers and indicates how a pulse broadens as it propagates within a material with an uncompensated dispersion (a non-zero GDD), and GDD becomes increasingly important for shorter pulses (corresponding to a large spectral bandwidth). In the case of the optical and NIR spectral regions, dispersion compensation in femtosecond lasers is readily accomplished with internal or external elements such as prisms, grating or chirped mirrors that introduce a GDD that is opposite to that of the laser medium. This brings the overall GDD down to zero and limits the broadening of ultrashort pulses. Although THz dispersion compensation has been considered in the case of frequency comb generation via four wave mixing, no studies have been applied to active mode locked QCLs for stable short pulse generation. [17,18]

In this paper, we resolve the THz QCL short pulse bottleneck through a novel on-chip geometry that permits the GDD of the QCL to be compensated, leading to considerably shorter pulses when the QCL is active mode locked. [15,19] This is realized through the monolithic integration of a small resonator at one end of a 2.5 THz QCL cavity (shown schematically in figure 1(a)), based around a Gires-Tournois Interferometer (GTI) approach [23] that adds an opposite dispersion to that of the material. By judiciously designing the length of the integrated GTI, applying the GTI ‘off-resonance’, and exploiting the high reflectivity of the metal-metal QCL waveguide, [12] significant compensation of the QCL’s inherent GDD can be realized. This directly results in pulse durations as shorts as 4 ps, from 16 ps with a standard QCL geometry, with a continuous Gaussian spectral range extending from 2.3 to 2.9 THz. The dispersive effect of the GTI mirror is clearly demonstrated by characterizing a GTI of a length that results in zero dispersion compared with one that introduces too much dispersion. The former shows a stable ultra-short pulse train while the latter destroys the pulse formation. This is further confirmed

by characterizing the free running electrical beat note that show a very narrow linewidth for correctly dispersion compensated QCL. Finally, the same approach is applied to a 3.25 THz QCL to demonstrate the generality of the technique. A 5 ps pulse duration is generated whose frequency emission ranges from 3.1 THz to 3.4 THz. As the GTI is used ‘off-resonance’ and not in the typical ‘on-resonance’ case, this relatively simple approach can be easily scaled to compensate for even greater spectral bandwidths and potentially attain sub-picosecond pulse widths. [24] Indeed THz QCLs with spectral bandwidths exceeding 500 GHz (FWHM) have been demonstrated [17] and would be adapted to ultra-short THz pulse generation.

2. Laser design and experimental technique

A QCL with a LO phonon depopulation scheme was used, based on a 3.1 THz QCL that has been shown to operate up to 200K. [25] The design was modified to operate at lower frequencies (~ 2.5 THz) by increasing the well and barrier widths. Starting from the injection barrier, the well and barrier widths were $4.85/10.24/2.77/9.37/4.62/18.4$ nm ($\text{Al}_{13}\text{Ga}_{87}\text{As}$ barriers in italic). The 18.4-wide-nm well was n-doped at a level of $6 \times 10^{16} \text{ cm}^{-3}$ over the central 6 nm. The growth was performed using molecular beam epitaxy. The wafer was processed into MM waveguides using standard lithography with the ridge defined using ICP etching for a vertical ridge profile. The GTI was realized in the same processing step by etching through the active region at one end of the QCL ridge separated from the main QCL ridge by a small sub-wavelength ($\sim 1.5 \mu\text{m}$) air gap (see figure 1(b-c)). For all the experiments, QCLs are maintained at a working temperature of 20 K.

The pulse characterization of the THz quantum cascade laser (QCL) is based on coherent sampling of the electric-field (E-field) using electro-optic detection. Figure 1(d) shows a schematic of the experimental arrangement. This technique requires to phase lock the emission

of the THz QCL to a THz pulse, which in turn is locked to the repetition rate of a femtosecond laser. To fulfil this requirement, an established ultrafast injection seeding technique is employed. A broad-band THz pulse (seed) with a fixed phase is generated using a photoconductive switch excited by a femtosecond Ti: Sapphire laser. The THz seed pulse is injected into one end cavity of the QCL waveguide prior to gain switching the QCL with an electrical radio frequency (RF) pulse of 40 dBm with a duration of a few nanoseconds. This allows the THz input pulse to be amplified and eventually seed the QCL emission, instead of being initiated by the QCL's inherent spontaneous emission. To initiate the mode-locking regime, a microwave modulation of the QCL bias of 30 dBm is added close to the THz cavity round-trip frequency. The microwave modulation is generated from the photo-excitation of an ultrafast photodiode by a pick-off beam of the Ti:Sapphire laser. The generated electrical signal consists of a comb of frequencies extending to \sim 20 GHz separated by the Ti:Sapphire repetition rate (76 MHz). An yttrium iron garnet bandpass filter is used to pick out a harmonic of the reference laser repetition rate close to the QCL cavity round-trip frequency, which is then amplified by a set of microwave power amplifiers. Further details of the technique can be found in References [26] and [16].

3. Dispersion compensation and GTI

When dealing with mode-locked broadband THz QCLs and short pulse generation, GDD management is challenging due to several factors. Firstly, the material GDD (i.e the index dispersion related to the material) owing to bulk GaAs is an important factor as a result of the residual absorption from the Reststrahlen band. [17,18] Secondly, gain GDD is even greater than material GDD owing to the dispersion added by the intersubband transition and can significantly limit THz frequency comb operation. [17] Thirdly, in contrast to optical and near infrared frequencies, there is a lack of dispersion compensation schemes for THz wavelengths. In fact, there are only a few concepts available to reduce the total GDD. Schemes that have

been applied to THz QCL waveguides have used chirped waveguides to show frequency comb operation through four wave mixing. [18,27] Although impressive results have been shown with octave spanning spectrum, no stable pulse generation has been demonstrated as the four-wave mixing process results in a frequency modulated spectrum. Flat dispersion can also be engineered into the QCL active region through a flat gain profile that permits frequency comb generation. [17] Indeed recently this technique has been shown to generate single pulses of duration 2.5ps. [28] However, importantly the pulses generated were not stable, a fundamental criteria for the application of any short pulse laser system, with pulses widening after only a single round-trip amongst the three pulses presented. (Unstable pulses as shorts as 3ps with narrower bandwidth QCLs have been generated previously [19] when a QCL is not mode locked). THz dispersion management has also been considered for passive waveguides. [29]

A GTI is a compensation scheme that is used in the optical and near-infrared domain to compress pulses. [30] It has also been applied to frequency comb generation in mid-infrared QCLs. [31] A regular GTI generally consists of a small resonator realized using dielectric coatings (of length typically on the same order as the wavelength of the laser in the material) operating in reflection where, in the ideal case, the front mirror is of low reflectivity ($r_1^2 \sim 0.1$) while the back mirror is perfect ($r_2^2 = 1$) (see figure 1(a) for a schematic). (Here r_i corresponds to the *field* reflectivities). The reflectivity is unity over the entire frequency range, but the phase is strongly frequency dependent owing to the small cavity acting as a Fabry-Pérot resonator. This gives rise to both positive and negative group GDD given by : [23]

$$GDD = - \frac{2\tau^2(1-r_1)\sqrt{r_1} \sin(\omega\tau)}{(1+r_1-2\sqrt{r_1} \cos(\omega\tau))^2} \quad (1)$$

where $\tau=2n_g l/c$ denotes the round trip time of the GTI where n_g is the group refractive index, the speed of light in vacuum c and the length of the GTI l . By choosing the length of the

resonator correctly, a compensation of the material and gain dispersion can be achieved. For example, GTIs have been operated in the negative GVD regime in order to compensate for excess positive GDD in picosecond mode-locked Ti:Sapphire lasers. [30] The GTI mirror in the optical range is normally realized using dielectric coatings with thicknesses on the order of the wavelength. However, for the THz range where the wavelength is typically 100 μm, thick dielectric coatings to realize the reflectivity conditions are extremely difficult to fabricate. In this work, rather than depositing a dielectric, we use the QCL itself and the confinement of the electromagnetic mode to realize a monolithic GTI. Although the reflectivities are different from the ideal case significant dispersion compensation can still be achieved.

In detail, by etching a small air gap ($\sim 1.5 \mu\text{m}$) into the MM waveguide to realize a small cavity at the end of the QCL (see figure 1 (b-c)), this results in a GTI with a contrast in the reflectivities of the front and back mirror. Using a finite-difference-time-domain method (Meep software package, see supplementary material S1), the GTI realized in this work is calculated to have a front reflectivity of $r_1 = 0.61$ and a back mirror reflectivity of $r_2 = 0.83$ (the latter a result of the strong confinement of the metal-metal waveguide mode) and thus different from the ideal case. Consequently, the well-established formula for the GDD introduced by a perfect GTI needs to be generalized in order to take account of the non-unity reflection coefficient of the second mirror. The GDD is the second derivative of the spectral phase with respect to the angular frequency and the general expression for the spectral phase of a GTI with a non-unity reflection coefficient is :

$$\Phi_{qGTI} = \arctan \left(\frac{r_1^2 \sin(\omega\tau) - \sin(\omega\tau)}{\frac{r_1}{r_2} + r_1 r_2 \cos^2(\omega\tau) - r_1^2 \cos(\omega\tau) + r_1 r_2 \sin^2(\omega\tau) - \cos(\omega\tau)} \right) \quad (2)$$

Here n is taken as the refractive index of GaAs. The effect of r_1 being considerably higher with respect to the ideal case results in more pronounced variations of the GDD near the resonant

frequencies but with little effect off-resonance, where we operate our GTI. (Further details of the calculation and simulations are detailed in the supplementary material S1).

Figure 2(a) shows the individual GDD contributions from the GTI (with 58 μm and 38 μm lengths that are used in the experiments), the GaAs material, and the gain (3 mm long cavity). (The waveguide dispersion is considerably smaller than the gain and material [17]). The material GDD is obtained from the dispersion relation and the gain GDD is calculated from the Kramers-Kronig relation (see supplementary material). [17] The latter is modelled with a gain of 10 cm^{-1} with a frequency centered at 2.48 THz, full width at half maximum (FWHM) of 600 GHz. The gain GDD provides a zero-crossing at its center-frequency and clearly dominates over the positive GaAs material GDD. As depicted in figure 2(a), the GDD of the 58 μm GTI is mostly negative below the center-frequency of the gain (at 2.48 THz) and positive above it, opposite to the gain GDD. In contrast, a 38 μm GTI only provides negative GDD in the investigated region. An important point to note is that here the GTI is employed ‘off resonance’, that is between the resonance frequencies at ~ 2.25 THz and ~ 2.75 THz of the 58 μm GTI. This is in contrast to the typical application of GTIs, used ‘on-resonance’ that is inherently spectrally narrowband. [30] By applying the GTI off-resonance, a much large spectral bandwidth can be compensated. Indeed, shorter GTI off-resonance cavities have the potential of compensating bandwidths greater than 1 THz (see supplement information S1). Finally, figure 2(b) shows the gain and the material GDD compared to the total GDD (sum of material, gain and GTI GDD) with the GTI QCLs. Remarkably, the total GDD is approximately flat in the region from 2.4 to 2.7 THz for the 58 μm GTI around zero GDD, while it is entirely negative for the 38 μm GTI.

To summarize, a GTI with non-ideal reflectivities can be realized using the QCL material itself. By designing the correct length of the GTI (58 μm for emission around 2.5 THz), the GTI can

be used to compensate the dispersion induced by the gain profile and the material, and hence realize short pulses when mode locked. A broad bandwidth of the GDD compensation is achieved by exploiting the both the positive and the negative GDD regime of the ‘off-resonance’ GTI, thus compensating positive and negative gain GDD simultaneously.

4. Results

In this study, QCLs with a center lasing frequency designed to be ~ 2.5 THz with a large emission bandwidth close to 0.5 THz were used, based on a modified LO phonon depopulation active region operating at 2.7THz. Two QCLs with short GTI cavity lengths of 58 μm and 38 μm are realized. The ridge width for both devices was 68 μm and the total length of the cavity was ~ 3.2 mm. A 3 mm long standard QCL (i.e. without the GTI) was also realized with a ridge width of 68 μm . The light-current density-voltage (LJV) characteristics for both devices are shown in figure 3a. The output power was measured using a pyroelectric detector. The LJV characteristics are similar showing that the GTI does not affect the QCL performance. It should be noted that the GTI is used as a passive element without applied bias in all the results presented, where no intersubband absorption is expected at the lasing frequency owing to the LO phonon depopulation design.

Prior to mode locking, the free running (i.e. no active modulation) spectra were taken in the injection seeding regime. A quasi-DC bias of 0.62 kA.cm^{-2} and 0.6 kA.cm^{-2} are applied to the GTI and standard QCL, respectively. This is combined with the RF modulation described above. Figure 3(b) shows the amplitude spectra for the standard QCL showing emission between 2.1 THz and 2.7 THz. The spectral bandwidth of the GTI QCL was similar. An enhanced view of the spectra is shown in figure 3(c). As can be observed the spacing of the modes is different for each sample. The free spectral range (i.e. the separation between Fabry-Perot modes) was

measured to be 13.4 GHz and 12.9 GHz for the standard and GTI QCLs, respectively. No evidence of higher order modes were observed, possibly owing to the top metal setback when compared to the ridge [28]. (The spectra are taken using the injection seeding technique that permits coherent detection of the QCL emission). [26]

The microwave modulation close to the round-trip frequency is added to the injection seeding technique to actively mode lock the QCL such that short pulses are generated i.e. to fix the frequency spacing and the phase of each mode. [16] The microwave power is set to 30 dBm. The microwave modulation frequency that resulted in the clearest pulses was 12.62 GHz and 12.88 GHz for the standard and GTI QCL samples, respectively. It is important to note that for the standard QCL, the modulation applied is considerably different to the free spectral range. This has been observed previously and is discussed further below regarding the spectral response and the uncompensated dispersion. [19] In figure 4, the electric field emission as a function of time of the 58 μ m GTI QCL (red trace (a)) and the standard QCL (black trace (b)) are compared. (The 58 μ m GTI is designed to provide negative and positive dispersion compensation of the THz QCL emission as shown in figure 2). As it can be clearly seen, after an initial amplification stage ($t < 500$ ps), stable pulses are formed and the insertion of a dispersion compensation permits the pulse duration of the GTI QCL to be greatly reduced compared to the standard QCL.

Figure 4(c) and 4(d) shows a zoom of one pulse for the GTI and standard QCL, respectively, highlighting strongly the difference between the two cases. Considerably fewer electric field oscillations are observed for the GTI QCL, comparable to that of standard ultrafast femtosecond lasers in the optical domain. To extract the FWHM of the pulse duration, a Gaussian fit is used to approximate the pulse shape intensity as shown in the dashed green line in figure 4(e) and

(f). Figure 4(g) is a comparison of the pulse FWHM with and without the GTI (triangle and rectangle scatter, respectively) as a function of the THz cavity round trip time. Before reaching the steady state, the pulses broaden during the laser E-field built-up time (before 500 ps corresponding to six round trip times of the THz pulse). In fact, directly after the QCL is gain switched in the active mode locking regime, the pulse can be as short as 2.3 ps (9.6 ps) for the QCL with (without) GTI. This is a result of the broadband seed and the entire gain bandwidth being amplified in this transient range. [32] Once in the steady state regime, a stable pulse train is observed. The pulses duration reaches a value of \sim 4 ps for the QCL with the GTI. This is more than 4 times shorter than the stabilized pulse duration of the standard QCL (\sim 16 ps). (This latter value is longer than a previous demonstration of 11 ps as the active region here is modified to operate at lower frequencies). [19]

The effect of these shorter pulses can also be observed in the spectra. In figure 5(a) and 5(b), the spectral intensity with and without the GTI, respectively, from the entire 1 ns time scan (1 GHz resolution), as well as the spectral phase dependency of the QCL emission within a single pulse (blue line) are shown. These are determined from the Fourier transform of the QCL E-field of figure 4. Even though both cases present similar spectral bandwidth to that without the active modulation (see figure 3), the QCL with the GTI has a considerably better distribution of the longitudinal modes and a continuous Gaussian spectrum with the emission frequency ranging from 2.3 to 2.8 THz, illustrating the effect of dispersion compensation. We also observe a shift towards higher frequencies for the GTI QCL when compared to the standard QCL. This is in agreement with the simulations of figure 2 that show a flat total GDD at frequencies blue shifted from that of the gain GDD profile. An indication of the effect of dispersion can also be deduced by analyzing the frequencies applied to achieve pulse behavior. In the case of the GTI QCL, as the dispersion is flatter, the microwave modulation needed to fix the phase and mode

separation is approximately the same as the free spectral range. However for the standard QCL, a considerably different frequency is used compared to the free spectral range (12.62 GHz instead of 13.4 GHz). This implies that the microwave modulation is compensating for the dispersion. (The dispersion is greater the further away from the zero crossing of the gain GDD, see figure 2). This also explains the spectral shape of the standard QCL as the difference between the free spectral range and the applied microwave modulation limits the number of modes that can be brought above threshold resulting in a narrower spectrum for the standard QCL around the central frequency. The two set of enhanced modes seen around 2.25 THz and 2.65 THz are a result of the modulation of 12.62 GHz coinciding with the free running Fabry-Perot modes of the cavity (see supplementary material for a comparison between the free running and mode locked QCL).

The spectral phase analysis of the pulses permits the role of dispersion to be further elucidated in our devices. As mentioned above in the simulations of the GDD, the second derivative of the spectral phase needs to be equal to zero over the range of laser frequencies to permit short pulse generation when active mode locked. Equivalently, the spectral phase should have a linear behavior. As we measure the time resolved electric field, the spectral phase can be easily accessed. For the standard QCL, a change in the slope of the spectral phase is observed between the different lasing bands around 2.25 THz, 2.5 THz and 2.65 THz (blue curve figure 5 (a)). This indicates that all the modes are not locked leading to the formation of longer pulses i.e. the active modulation by itself is not able to compensate the entire QCL bandwidth dispersion. At best, a GDD compensation can be observed between \sim 2.4 THz to \sim 2.55 THz. The situation is entirely different for the QCL with the GTI. The spectral phase between 2.31 THz and 2.86 THz is linear, indicating that the dispersion is almost zero and that all the modes are locked by the gigahertz modulation. This leads to the continuous spectrum where all the modes are equally

spaced by the gigahertz modulation frequency (\sim 12.8 GHz). Therefore with the correctly chosen length of the GTI, more than 0.55 THz QCL bandwidth emission is dispersion compensated for a QCL with central frequency of \sim 2.55 THz. The FWHM is 0.15 THz and taking a Gaussian form of the pulse, the Fourier bandwidth limited pulse width is expected to be 2.9 ps. This suggests a small mismatch between the GDD of the GTI with the gain GDD.

To further evaluate the dispersion compensation technique, we also characterized the pulse behavior of the THz QCL with 38 μm GTI. This length should lead to a negative dispersion compensation within the full THz emission range of the laser (see figure 3(b)), wiping out the short pulse behavior. In figure 6(a), the temporal profile of the electric field is shown for QCLs with a 38 μm GTI (top part) and the 58 μm GTI detailed previously (bottom part) with the active modulation. For both cases, the black curve shows the superimposed gigahertz modulation (12.119 GHz for the 38 μm and 12.886 GHz for the 58 μm GTI, frequencies close to the electrical beat note of each QCL). Only the positive component of the sine wave is represented for clarity. As can be seen, the THz pulses of the QCL with 58 μm GTI are perfectly in phase with the phase velocity of the gigahertz wave as a function of the cavity round trip time. In the case of the 38 μm length GTI, no clear and stable pulse behavior is observed. However, the effect of the negative GDD on time evolution of several pulses (with two highlighted in green and orange arrows) can be observed directly as function of the cavity round trip time. For each round trip, the two pulses are delayed by approximately 4.5 ps. As the pulses are not in-phase with respect to the maximum of the sine wave modulation, they encounter less amplification. Therefore owing to the large negative GDD introduced by the 38 μm GTI, rather than generating short THz pulses, it prevents the pulses to merge. Finally, to confirm the poor performance of the 38 μm GTI, the free running electrical beat notes are recorded just above threshold, where the active mode locking technique is applied (\sim 0.7 kA/cm²). [19] The beat

note signature of the QCL with a 58 μm GTI (Figure 6(b)) is 10 times narrower than the QCL with 38 μm GTI (Figure 6(c)), indicating a lower overall dispersion for the former.

The universality of this dispersion compensation approach can be shown by applying the concept to other frequencies with the GTI length designed accordingly. As demonstrated above, the dispersion compensation needs to operate close to the zero crossing point of the GTI GDD. In Figure 7, a 3.25 THz QCL, with a hybrid active region design and a 3 mm length cavity, is used to demonstrate the broad application of the technique for pulse compression. [33] This GTI QCL presents much lower current threshold. For this case, a quasi-DC bias below threshold of 0.2 kA.cm⁻² is applied. The GTI length integrated to the 3.25 THz QCL is chosen to be 19.5 μm such that the zero crossing point of its GDD is near the center lasing frequency of the THz QCL (3.2 THz, green curve in figure 7(d)). Figure 7(a) shows the QCL electric field emission when such a device is free-running (no microwave modulation, black) and active-mode locked (magenta) at a modulation frequency of 12.3 GHz (close to the electrical beat note). Figure 7(b) is a zoom of one of the pulse showing that the E-field is fully sampled. Figure 7(a) shows stable and short pulse formation with the pulse intensity very close to a Gaussian shape with a FWHM of ~ 5 ps (see figure 7(c)). (Interestingly, although not entirely stable in time, pulse behavior is already observed in the free running case showing the effect of dispersion compensation). Taking the Fourier transform of figure 7(a), the corresponding FWHM of the spectrum bandwidth is found to be ~ 0.10 THz (figure 7(d)). As observed previously, in the mode-locking regime, the modes are exalted leading to a Gaussian intensity distribution when compared to the QCL spectrum without the gigahertz modulation (figure 7(e)). The Fourier bandwidth limited pulse width for 0.10 THz is expected to be 4.4 ps. Therefore, with an integrated GTI, pulses are generated close to the bandwidth-limited case.

5. Conclusion

Our experimental results show a dispersion compensation scheme, monolithically integrated into the THz QCL waveguide, can be successfully engineered to greatly shorten the pulse duration of THz QCLs when active mode locked. It is based on an adapted GTI concept where a small resonator possesses non-equal cavity mirror reflectivities, permitting control of the total dispersion. For an integrated GTI, the high facet reflectivity of a QCL embedded in a MM waveguide is used as the back end mirror for the THz pulse while the low reflectivity mirror is realized by etching a sub-wavelength air gap directly in the waveguide. By designing the GTI's length to compensate the QCL dispersion around its central frequency, and operating the GTI 'off-resonance', pulse durations as short as 4 ps can be formed. This technique of on-chip dispersion overcomes previous bottlenecks to realize stable short pulses from THz QCLs. Further, as the GTI is applied 'off-resonance', it has the potential to compensate even greater bandwidths that would allow shorter pulse widths to be achievable (see supplementary material). Such short pulses would be of interest to replace Ti:Sapphire lasers for short THz pulse generation, THz frequency comb generation [17,18,27], and dual frequency comb spectroscopy where the mode spacing can be actively controlled with stable microwave generators rather than passive techniques that are currently employed. [34–36]

Supporting Information

See supplementary material

Acknowledgements

FW, HN, VP, SH performed the experiments, TF, HN, SM, NJ contributed to the data interpretation and performed the theoretical development and simulations. MA, CS, SM and RC performed the device design and realization. LHL, EHL and AGD performed the growth of

the samples. FW, HN, NJ, AGD, JM, JT, SSD wrote and developed the paper. FW, SSD contributed to the original scheme.

The authors acknowledge funding from European Union FET-Open grant ULTRAQCL 665158, ANR-12-NANO-0014 “PhaseLock”, the EPSRC (UK), the EC programme (TOSCA), ERC “GEM” grant, the Royal Society and Wolfson Foundation and the Conseil Général de l’Essonne.

Keywords: Quantum cascade laser, Terahertz, Active mode-locking, Gires-Tournois interferometer, Short pulse generation

References

- [1] M. Tonouchi, Nat. Photonics **1**, 97 (2007).
- [2] M. Ravarò, V. Jagtap, G. Santarelli, C. Sirtori, L. H. Li, S. P. Khanna, E. H. Linfield, and S. Barbieri, Appl. Phys. Lett. **102**, 091107 (2013).
- [3] P. Dean, A. Valavanis, J. Keeley, K. Bertling, Y. L. Lim, R. Alhathloul, A. D. Burnett, L. H. Li, S. P. Khanna, D. Indjin, T. Taimre, A. D. Rakić, E. H. Linfield, and A. G. Davies, J. Phys. Appl. Phys. **47**, 374008 (2014).
- [4] L. Consolino, A. Taschin, P. Bartolini, S. Bartalini, P. Cancio, A. Tredicucci, H. E. Beere, D. A. Ritchie, R. Torre, M. S. Vitiello, and P. De Natale, Nat. Commun. **3**, 1040 (2012).
- [5] S. Bartalini, L. Consolino, P. Cancio, P. De Natale, P. Bartolini, A. Taschin, M. De Pas, H. Beere, D. Ritchie, M. S. Vitiello, and R. Torre, Phys. Rev. X **4**, (2014).
- [6] K. Kawase, Y. Ogawa, Y. Watanabe, and H. Inoue, Opt. Express **11**, 2549 (2003).
- [7] I. Amenabar, F. Lopez, and A. Mendikute, J. Infrared Millim. Terahertz Waves **34**, 152 (2012).
- [8] A. Garnache, S. Hoogland, A. C. Tropper, I. Sagnes, G. Saint-Girons, and J. S. Roberts, Appl. Phys. Lett. **80**, 3892 (2002).
- [9] B. W. Tilma, M. Mangold, C. A. Zaugg, S. M. Link, D. Waldburger, A. Klenner, A. S. Mayer, E. Gini, M. Golling, and U. Keller, Light Sci. Appl. **4**, e310 (2015).
- [10] A. H. Quarterman, K. G. Wilcox, V. Apostolopoulos, Z. Mihoubi, S. P. Elsmere, I. Farrer, D. A. Ritchie, and A. Tropper, Nat. Photonics **3**, 729 (2009).
- [11] R. Köhler, A. Tredicucci, F. Beltram, H. E. Beere, E. H. Linfield, A. G. Davies, D. A. Ritchie, R. C. Iotti, and F. Rossi, Nature **417**, 156 (2002).
- [12] B. S. Williams, Nat. Photonics **1**, 517 (2007).

- [13] N. Jukam, S. S. Dhillon, D. Oustinov, J. Madeo, C. Manquest, S. Barbieri, C. Sirtori, S. P. Khanna, E. H. Linfield, A. G. Davies, and J. Tignon, Nat. Photonics **3**, 715 (2009).
- [14] M. S. Vitiello and A. Tredicucci, IEEE Trans. Terahertz Sci. Technol. **1**, 76 (2011).
- [15] S. Barbieri, M. Ravaro, P. Gellie, G. Santarelli, C. Manquest, C. Sirtori, S. P. Khanna, E. H. Linfield, and A. G. Davies, Nat. Photonics **5**, 306 (2011).
- [16] J. R. Freeman, J. Maysonnave, H. E. Beere, D. A. Ritchie, J. Tignon, and S. S. Dhillon, Opt. Express **21**, 16162 (2013).
- [17] M. Rösch, G. Scalari, M. Beck, and J. Faist, Nat. Photonics **9**, 42 (2014).
- [18] D. Burghoff, T.-Y. Kao, N. Han, C. W. I. Chan, X. Cai, Y. Yang, D. J. Hayton, J.-R. Gao, J. L. Reno, and Q. Hu, Nat. Photonics **8**, 462 (2014).
- [19] F. Wang, K. Maussang, S. Moumdji, R. Colombelli, J. R. Freeman, I. Kundu, L. Li, E. H. Linfield, A. G. Davies, J. Mangeney, J. Tignon, and S. S. Dhillon, Optica **2**, 944 (2015).
- [20] D. G. Revin, M. Hemingway, Y. Wang, J. W. Cockburn, and A. Belyanin, Nat. Commun. **7**, 11440 (2016).
- [21] C. Y. Wang, L. Kuznetsova, V. M. Gkortsas, L. Diehl, F. X. Kärtner, M. A. Belkin, A. Belyanin, X. Li, D. Ham, H. Schneider, P. Grant, C. Y. Song, S. Haffouz, Z. R. Wasilewski, H. C. Liu, and F. Capasso, Opt. Express **17**, 12929 (2009).
- [22] A. E. Siegman, *Lasers* (Mill Valley, Calif. : University Science Books, 1986).
- [23] F. Gires and P. Tournois, C R Acad Sci Paris **258**, 6112 (1964).
- [24] S. A. Diddams, D. J. Jones, J. Ye, S. T. Cundiff, J. L. Hall, J. K. Ranka, R. S. Windeler, R. Holzwarth, T. Udem, and T. W. Hänsch, Phys. Rev. Lett. **84**, 5102 (2000).
- [25] S. Fathololoumi, E. Dupont, C. W. I. Chan, Z. R. Wasilewski, S. R. Laframboise, D. Ban, A. Mátyás, C. Jirauschek, Q. Hu, and H. C. Liu, Opt. Express **20**, 3866 (2012).
- [26] D. Oustinov, N. Jukam, R. Rungsawang, J. Madéo, S. Barbieri, P. Filloux, C. Sirtori, X. Marcadet, J. Tignon, and S. Dhillon, Nat. Commun. **1**, 1 (2010).
- [27] J. Faist, G. Villares, G. Scalari, M. Rösch, C. Bonzon, A. Hugi, and M. Beck, Nanophotonics **5**, (2016).
- [28] D. Bachmann, M. Rösch, M. J. Süess, M. Beck, K. Unterrainer, J. Darmo, J. Faist, and G. Scalari, Optica **3**, 1087 (2016).
- [29] T. Fobbe, S. Markmann, F. Fobbe, N. Hekmat, H. Nong, S. Pal, P. Balzerwoski, J. Savolainen, M. Havenith, A. D. Wieck, and N. Jukam, Opt. Express **24**, 22319 (2016).
- [30] J. D. Kafka, M. L. Watts, and J.-W. J. Pieterse, IEEE J. Quantum Electron. **28**, 2151 (1992).
- [31] G. Villares, S. Riedi, J. Wolf, D. Kazakov, M. J. Süess, P. Jouy, M. Beck, and J. Faist, Optica **3**, 252 (2016).
- [32] J. Maysonnave, K. Maussang, J. R. Freeman, N. Jukam, J. Madéo, P. Cavalié, R. Rungsawang, S. P. Khanna, E. H. Linfield, A. G. Davies, H. E. Beere, D. A. Ritchie, S. S. Dhillon, and J. Tignon, Opt. Express **20**, 20855 (2012).
- [33] M. I. Amanti, G. Scalari, R. Terazzi, M. Fischer, M. Beck, J. Faist, A. Rudra, P. Gallo, and E. Kapon, New J. Phys. **11**, 125022 (2009).
- [34] S. Schiller, Opt. Lett. **27**, 766 (2002).
- [35] M. Rösch, G. Scalari, G. Villares, L. Bosco, M. Beck, and J. Faist, Appl. Phys. Lett. **108**, 171104 (2016).
- [36] Y. Yang, D. Burghoff, D. J. Hayton, J.-R. Gao, J. L. Reno, and Q. Hu, Optica **3**, 499 (2016).

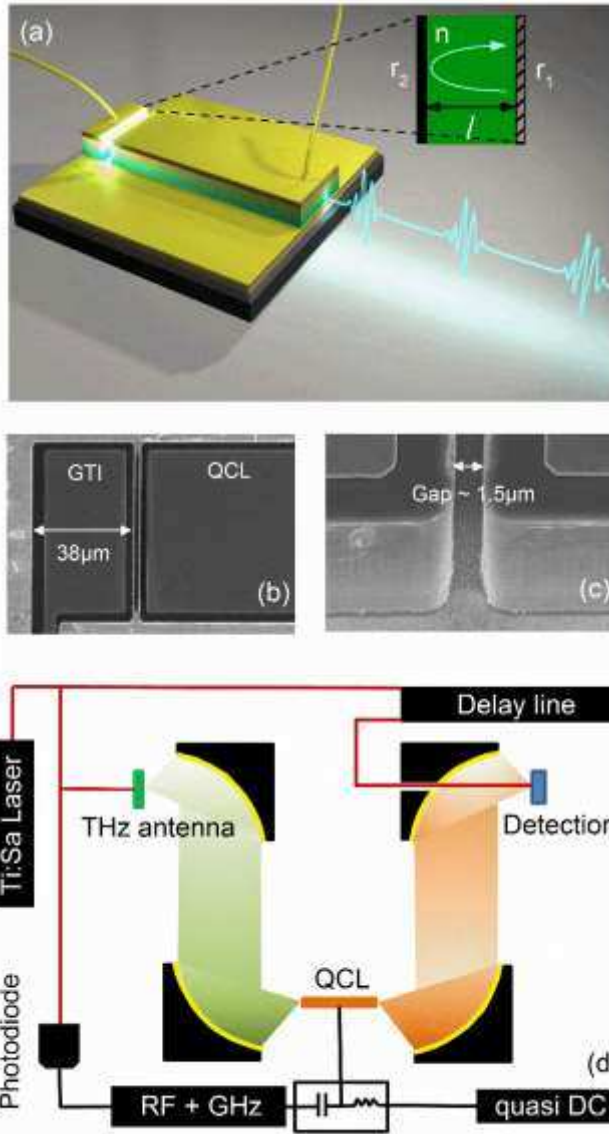


Figure 1. GTI and experimental schematic a) Schematic of the GTI coupled to a QCL to realise ultrashort THz pulses. The inset represents the GTI with asymmetric reflectivities, r_1 and r_2 , and a cavity length, l . b) SEM image of one end of the ridge showing the GTI coupled to the QCL cavity c) Magnified SEM image of the gap separating the GTI and the QCL. d) Schematic of the experimental arrangement to measure QCL pulse generation. The label ‘detection’ refers to a 500 μm ZnTe crystal for electro-optic sampling of the QCL E-field. Here, a THz pulse (green) generated from a THz antenna is used to seed the QCL emission (red) to permit phase resolved detection of the QCL field. The THz pulse is synchronized with an RF square wave and microwave modulation for the injection seeding technique.

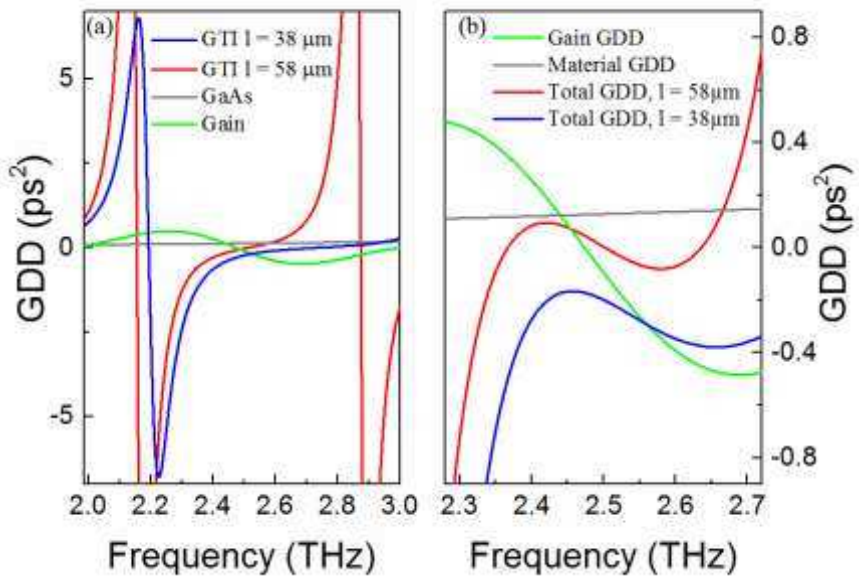


Figure 2: Group Delay Simulations of the gain, material and GTI. a) The individual GDD contributions of the GTI, bulk GaAs (grey) and the QCL gain (green curve). The GTI GDD is shown for a 58 μm (red) and 38 μm (blue curve) length cavity. b) The total GDD - GTI, material and gain - for a 58 μm (red) and 38 μm (blue curve) length GTIs. The contribution of the gain and material GDD is also shown for comparison (green and grey curves).

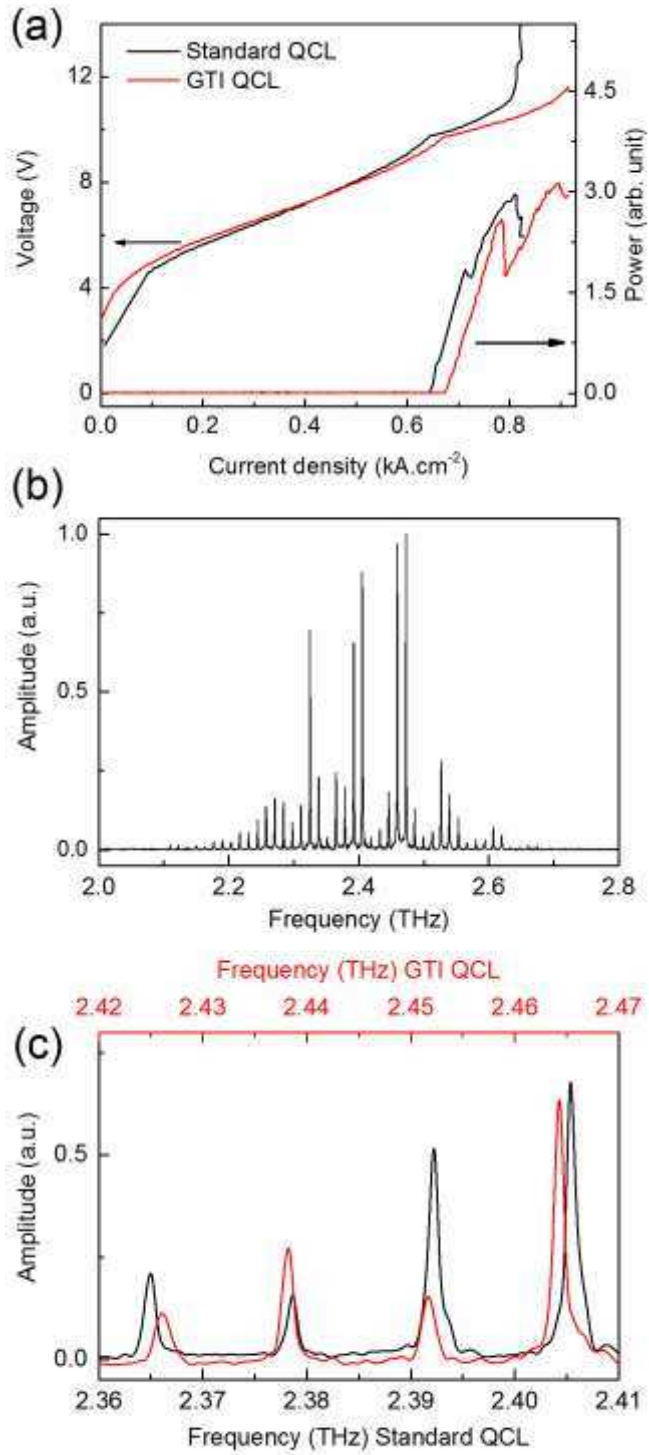


Figure 3: Free running spectral characteristics. (a) Light-current density-voltage (LVJ) characteristics of a GTI QCL as compared to the standard QCL. (b) Laser spectrum of the standard 2.5 THz QCL in a metal-metal geometry. (c) Enhance view of Fabry-Pérot modes of a GTI QCL (58 μm length, red line) as compared to a standard cavity one (black line).

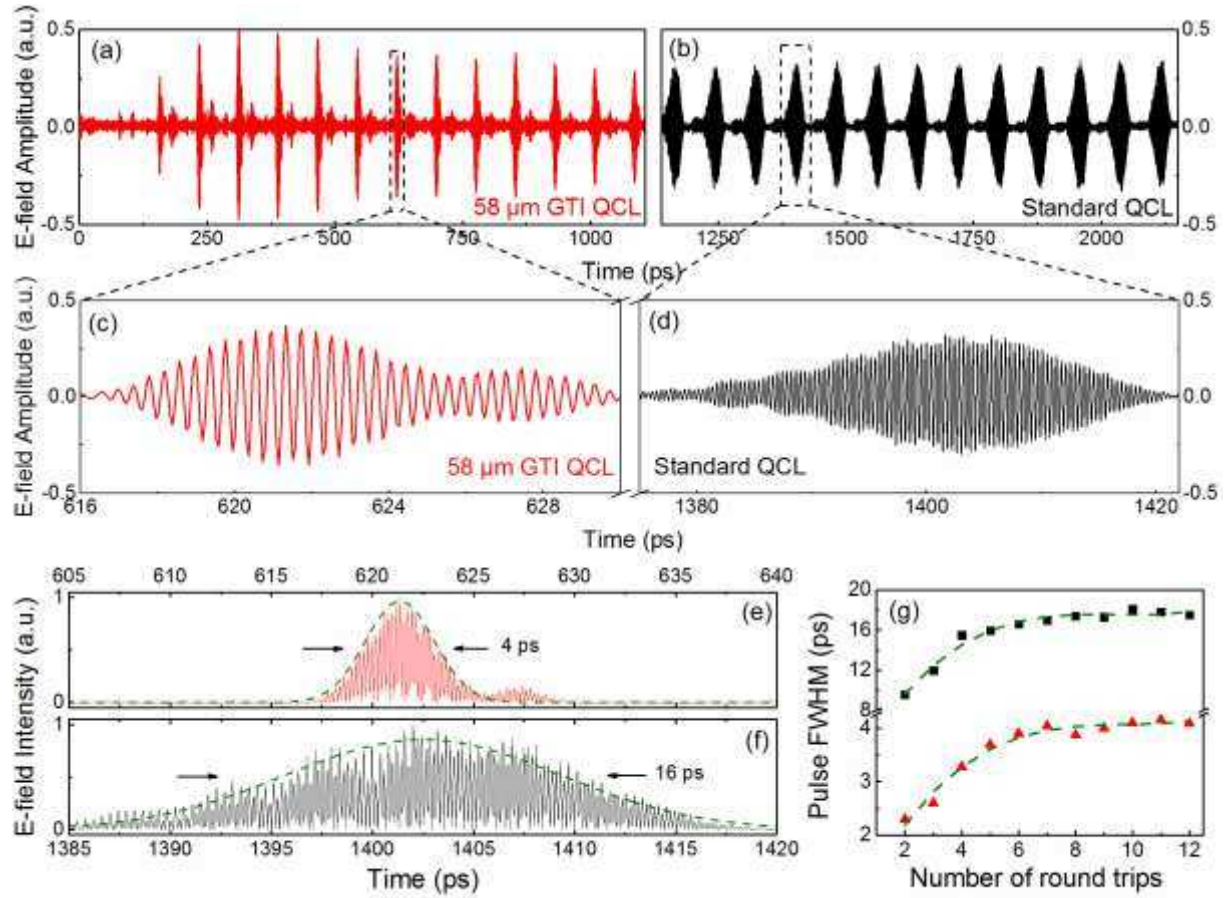


Figure 4: Pulse generation and time evolution of the THz QCL E-field. Pulse generation comparison of a QCL with a $58\text{ }\mu\text{m}$ GTI (red) and a standard QCL cavity (black). (a), (b) The active mode locked E-field as function of time for the QCLs, taken with a sampling step of 0.06 ps. A zoom of a single pulse is shown in (c) and (d) for both samples to highlight the resolved E-field oscillations. (Note the different time scales). (e), (f) show the E-field intensity for both samples with the FWHM calculated by fitting with a Gaussian shape (green curve). g) The FWHM of the pulses as a function of the number of cavity round trips for the QCLs. The green dashed line are eye guides.

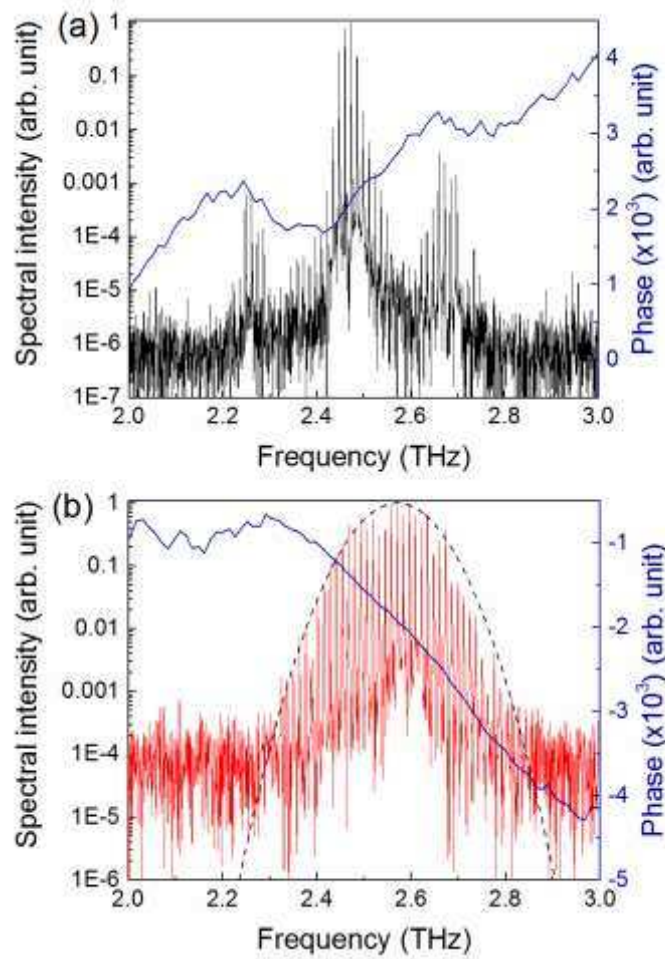


Figure 5: Active mode-locked QCL spectra and phase. The unwrapped phase of an individual pulse (blue line) for the active mode-locked QCL superimposed to the corresponding QCL spectrum for the standard QCL (a) and the QCL with 58 μm length GTI (b). The spectra are the Fourier transform of the QCL time response (power component) over a 1 ns scan length (1 GHz resolution).

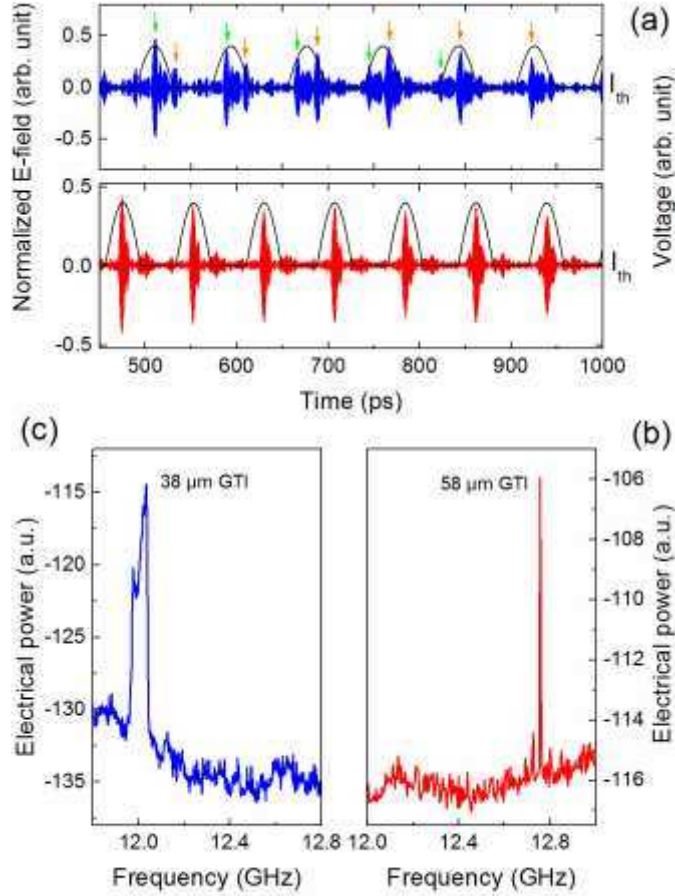


Figure 6: QCL active mode locked emission as a function of the GTI cavity size. (a) Electric field as a function of time generated for GTI length of 58 μm (bottom red) and 38 μm (top blue curve). The corresponding active GHz modulation (black lines) are superimposed to the QCL E-field emission. For clarity, only half the sinewave period is presented. The dephasing as a function of the THz round trip cavity between the THz pulses with respect to the active modulation for the 38 μm GTI is indicated with the green and the orange arrows. (b), (c) show the free running beat note close to laser threshold ($\sim 0.7 \text{ kA.cm}^{-2}$) for the QCLs with 58 μm and 38 μm GTIs, respectively.

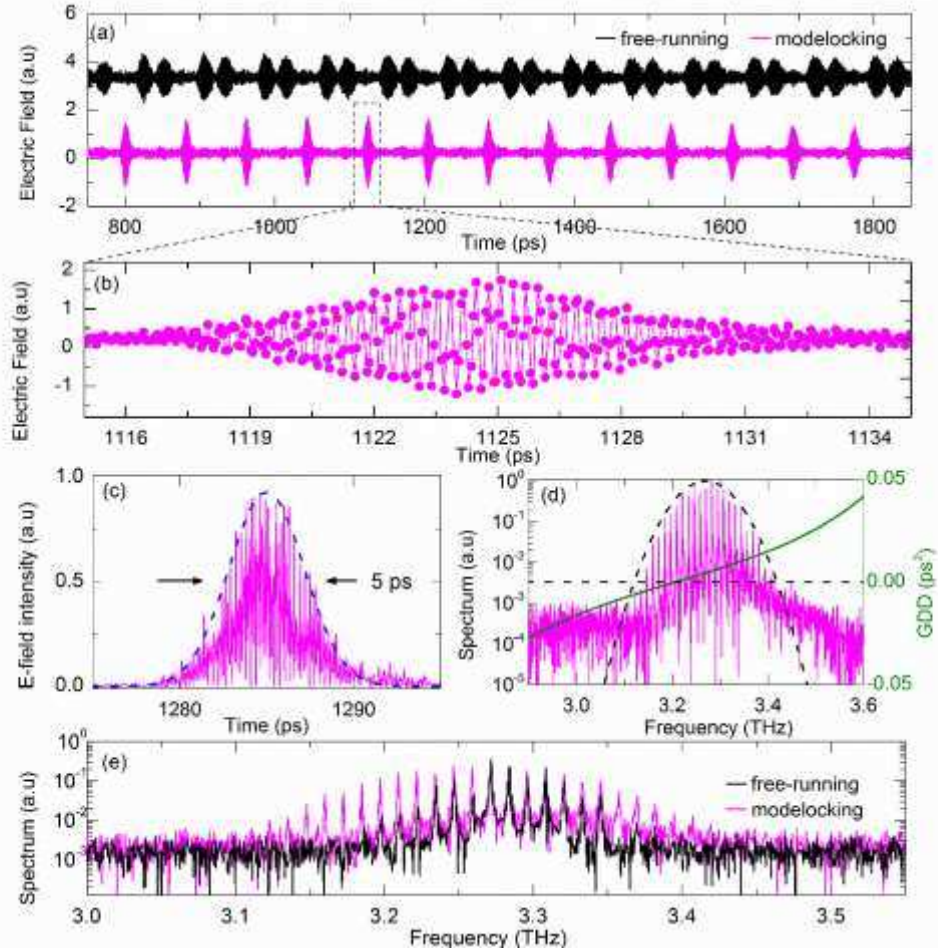


Figure 7: Short pulse generation from dispersion compensated 3.25 THz QCL. (a) The E-field as a function of time for the free running and active modelocked QCL coupled to a 19.5 μm length GTI. (b) Enhanced view of one pulse when QCL is active modelocked. Dots corresponds to the time resolution (c) Intensity time profile of one pulse when the QCL is active modelocked with the pulse duration ($\sim 5\text{ps}$) calculated from a Gaussian fit (blue line). (d) The active mode-locked intensity spectrum (FT of (a)) spanning the range from 3.1 to 3.4 THz. The green curve is the calculated GDD of the GTI with a zero-point crossing around 3.2 THz. (e) The amplitude QCL spectrum in free-running and active modulation conditions.